

ELECTRONIC SUPPLEMENTARY INFORMATION

Microstructure-driven annihilation effects and dispersive excited state dynamics in solid-state films of a model sensitizer for photon energy up-conversion applications

*Hossein Goudarzi,^a Loukas Koutsokeras,^b Ahmed H. Balawi,^c Chen Sun,^d Giorgos K. Manolis^{†, e}
Nicola Gasparini,^{c, f} Yuan Peisen,^b Giannis Antoniou,^b Stavros Athanasopoulos,^g Charalampos C.
Tselios,^h Polycarpos Falaras,^e Constantinos Varotsis,^h Frédéric Laquai,^c Juan Cabanillas-
González,^d Panagiotis E. Keivanidis^{b, *}*

^a Centre for Nano Science and Technology @PoliMi, Fondazione Istituto Italiano di Tecnologia, Via Pascoli 70/3, 20133 Milano, Italy

^b Device Technology and Chemical Physics Laboratory, Department of Mechanical Engineering and Materials Science and Engineering, Cyprus University of Technology, Limassol 3041, Cyprus

^c King Abdullah University of Science and Technology (KAUST), KAUST Solar Center (KSC), Physical Sciences and Engineering Division (PSE), Thuwal 23955-6900, Kingdom of Saudi Arabia

^d IMDEA Nanoscience, Calle Faraday 9, Ciudad Universitaria de Cantoblanco, Madrid, ES 28049, Spain

^e Institute of Nanoscience and Nanotechnology, NCSR “Demokritos”, 15341 Agia Paraskevi, Athens, Greece

^f Department of Chemistry and Centre for Processable Electronics, Imperial College London, W120BZ, UK

^g Departamento de Física, Universidad Carlos III de Madrid, Avenida Universidad 30, 28911 Leganés, Madrid, Spain

^h Environmental Biocatalysis and Biotechnology Laboratory, Department of Chemical Engineering, Cyprus University of Technology, Limassol 3603, Cyprus

† Deceased

AUTHOR INFORMATION

Corresponding Author: * Assoc. Prof. Dr. P. E. Keivanidis, e-mail: p.keivanidis@cut.ac.cy

Supplementary Information Contents

- Page 4: Materials and Methods
- Page 9: **Figure S.1**; Scanning Electron Microscopy imaging
- Page 10: **Figure S.2**; X-ray diffraction data on DPA powder and evaporated film
- Page 11: **Figure S.3**; Raman spectroscopy
- Page 12: **Figure S.4**; Composition-dependent grazing incidence X-ray diffractograms
- Page 13: **Figure S.5**; Grazing incidence X-ray diffractograms of PS:PtOEP 30 wt% and DPA:PtOEP 30 wt%
- Page 14: **Figure S.6**; Time-gated PL transients in the μs time scale
- Page 15: **Table S.1** and **Table S.2**; Fitting parameters of time-gate PL transients
- Page 16: **Figure S.7**; Time-gated PL spectra and Arrhenius plots of DPA phosphorescence
- Page 17: **Figure S.8**; Grazing incidence X-ray diffractograms, scanning electron microscopy imaging and time-gated PL spectra of PFO:PtOEP blend films
- Page 18: **Figure S.9**; Transient absorption ($\Delta T/T$) spectra of PS:PtOEP 6 wt% processed from toluene after photoexcitation at 540 nm
- Page 19: **Figure S.10**; Solvent-dependent UV-Vis and FT-IR spectra of DPA:PtOEP 2 wt% composites
- Page 20: **Figure S.11**; Solvent-dependent time-gated PL spectra of PS:PtOEP, DPA:PtOEP and PS:DPA:PtOEP films
- Page 21: **Figure S.12**; Fluence-dependent of the PtOEP triplet dimer PL emission intensity of PS:PtOEP, DPA:PtOEP and PS:DPA:PtOEP films developed from different solvents
- Page 22: References

Materials and Methods

Materials: The materials of this study were commercially purchased and used as they were received. The DPA and PS chemicals were purchased by Sigma-Aldrich, Inc. whereas PFO and PtOEP were purchased by American Dye Source, Inc. and Frontier Scientific, Inc., respectively.

Thin film preparation: All spin-coated blend films of PS:PtOEP, DPA:PtOEP, PS:DPA:PtOEP and PFO:PtOEP used in this study were prepared according to previously described solution-processing protocols [1-3]. The PS:PtOEP 6 wt% and PFO:PtOEP 6 wt% films used for transient absorption measurements were prepared by doctor blading PS:PtOEP and PFO:PtOEP from toluene solution on quartz substrates. Doctor blading was performed with a Zehntner ZAA 2300 doctor-blade unit under ambient conditions. Thermally evaporated DPA films were developed on glass/indium tin oxide (ITO)/ PEDOT:PSS substrates. The glass/ITO electrodes (XY15S, ITO substrates from Xin Yan Technology Ltd.) were ultrasonically cleaned using acetone and isopropanol for 15 min. After preliminary cleaning, the substrates were washed with Hellmanex III surfactant to remove contaminants and residues from the ITO surface. The substrates were again cleaned with deionized water followed by acetone and isopropanol for 15 min and soon after being placed in oxygen plasma (100 W power) for 10 min. A solution-processed hole-collecting interlayer of poly(3,4-ethylenedioxythiophene) polystyrene sulfonate (PEDOT:PSS, Merck, Clevios HTL Solar) was spin-coated at 3000 rpm for 1 min onto the ITO electrodes and thermal annealing was applied at 200 °C for 20 minutes. The glass/ITO/PEDOT:PSS electrodes were transferred in a N₂-filled glovebox (PureLabHE, Inert) and a thermal evaporator (Covap III, Angstrom Engineering Inc.) coupled to the N₂-filled glovebox was used for depositing DPA in

vacuum (4×10^{-8} mbar). A shadow mask was used for facilitating the formation of a DPA layer area of 0.8 cm^2 .

UV-Vis absorption characterization: UV-vis absorption spectra of the fabricated films were recorded with UV-2700 Shimadzu spectrophotometer operated in transmission mode. The absorption spectra of the PtOEP solution in toluene were also recorded and corrected after subtracting the absorption spectrum of pure toluene.

FT-IR characterization: FT-IR spectra were recorded using a Vertex 70v FTIR spectrometer (BRUKER) equipped with a photovoltaic MCT detector. Solid films were prepared by drop-casting of the respective solutions onto silver fluoride window. During spectra acquisition the sample compartment was purged with nitrogen gas. FT-IR spectra were registered in the $800\text{--}4000 \text{ cm}^{-1}$ spectral range at a 4 cm^{-1} resolution, and spectral signal was averaged from 100 scans.

Raman characterization: Micro-Raman analysis was performed using a dispersive Renishaw in-Via Reflex spectrometer. Raman spectra were registered in the $30\text{--}3200 \text{ cm}^{-1}$ range in a backscattering configuration following excitation by a near-infrared (NIR) diode laser emitting at 785 nm. The laser beam was focused onto the sample using a $\times 50$ long focal distance objective lens of a Leica DMLM microscope providing power density of approximately $1 \text{ mW } \mu\text{m}^{-2}$. The Raman scattered beam was filtered by a 30 cm^{-1} cutoff Rayleigh dielectric filter and analyzed through the 250 mm-focal length spectrograph, a 1200 lines/mm diffraction grating and a high-sensitivity deep depletion CCD detector. For each sample, 3-4 spots were taken, with an exposure time of 30 s and 2-10 accumulations. An internal Si reference was used for frequency shift calibration.

Scanning electron microscopy imaging: Scanning electron microscopy was used for the morphological evaluation of the spin-coated thin films. Prior to observation, the samples were

sputter coated with a thin metallic film to prevent charging and then loaded to a FEI Quanta 200 microscope. Secondary electron images were acquired at 5kV accelerating voltage and at various magnifications.

X-ray diffraction characterization: The x-ray diffraction (XRD) patterns were acquired in an Ultima IV (Rigaku) diffractometer equipped with a point detector (scintillator) and a Cu tube operated at 40 kV and 40 mA. The incident X-ray beam was configured in parallel mode by a set of multilayer curved mirror optics (CBO) and partially monochromatized (Cu K α , λ = 0.15418 nm). Powder samples were investigated by Bragg-Brentano geometry and patterns from thin films were acquired by asymmetric and out-of-plane scans, with a fixed incident theta angle between 0.5 – 1 °.

Time-integrated and time-gated gated photoluminescence characterization: Time-integrated and time-gated spectra of the studied systems were recorded at room temperature. The samples were photoexcited with the output of an optical parametric oscillator (Spectra-Physics VersaScan Midband 120) pumped by the third harmonic of a Nd:YAG Laser (Spectra-Physics INDI-40-10-HG) at 530 nm by a train of 10 ns pulses at a repetition rate of 10 Hz. No focal lens was used for the photoexcitation of the samples, and a laser spot size of 0.385 cm² was kept for all samples measured. The emitted light was dispersed in a spectrograph (Andor Shamrock Spectrograph, SR303i) with a 150 lines per millimeter grating and detected with a gated intensified charge-coupled device camera (Andor iCCD, iStar DH320T-25U-73). During the spectroscopic characterization, the samples were kept in a liquid-nitrogen variable-temperature cryostat (Janis VPF-100) that was evacuated by a turbomolecular pump (Pfeiffer TSH 071E Economy Dry Vacuum Pumping Station) so that a dynamic vacuum of a typical pressure of 10⁻⁷ mbar was

maintained during the measurements. Photoexcitation intensity-dependent measurements were performed by using the combination of a set of neutral density (ND) filters of known transmittance values at 532 nm. For each ND filter combination, the laser pulse energy was determined with a Field MaxII-TOP (Coherent Inc.) reader unit equipped with a Coherent J-10MB-HE pyroelectric energy sensor.

Time-resolved Streak camera photoluminescence characterization: The time-resolved PL (TR-PL) spectra of PFO:PtOEP were acquired with a streak camera set-up. The films were kept sealed in nitrogen environment and were photoexcited at 532 nm by a pulsed Helios laser (1 ns pulse length) with a repetition rate of 1 kHz. Photoexcitation of the samples occurred without using a focal lens in order to avoid thermal effects and photoluminescence was collected by an optical telescope (consisting of two plano-convex lenses), focused on the slit of a spectrograph (PI Spectra Pro SP2300). The photoexcitation spot was 0.14 cm², as determined by a LaserCam-HR11-2/3” camera system (Coherent). The average optical power of the incoming laser was regulated between 3 – 90 mW with a combination of ND filters of known transmittance values at 532 nm. For each ND filter combination, the laser power was determined with a Coherent LabMax TOP reader unit equipped with a Coherent OP-2-VIS thermopile sensor. Acquisition of the TR-PL data was enabled in the 10 ns time range by a C10910 Hamamatsu streak camera in slow single sweep mode in combination with a M10913 unit.

Transient absorption characterization: Transient absorption measurements were carried out with a Clark-MXR CPA-1 regenerative amplifier, which delivered pulses at 775 nm (1 kHz, 120 fs, 1 mJ). The primary beam was split into pump and probe beams. Pump pulses centered at 540 nm were generated with home-built two stage non-collinear optical parametric amplifier and attenuated to adjust the excitation density. Broadband supercontinuum pulses were instead

generated by focusing a portion of the fundamental onto a CaF₂ crystal to generate a white light continuum beam from 300–750 nm by self-phase modulation and the pump-probe delay line was computer-controlled. Both pulses were temporally and spatially overlapped on the sample. The pump spot size was with a radius of 85 μm, much lower than the radius of the probe spot size. Probe pulses transmitted through the sample were sent to a prism spectrometer (Entwicklungsburo Stresing GmbH) equipped with a double CCD line array. The second array allowed to record probe pulses which did not pass through the sample (reference) to obtain the transmission spectra with and without pump (T* and T). A customized homemade software recorded the normalized change in transmission ($\Delta T/T$) for each single shot. All the measurements were performed with pump and probe polarization set at the magic angle (54.7°) by adjusting the polarization angles with half-wave plates. Samples were placed in a vacuum chamber (10⁻³ mbar) equipped with quartz windows to measure transmission.

Density functional theory: The molecular Raman spectrum of DPA was computed by using density functional theory (DFT) calculations. The hybrid B3LYP exchange-correlation functional with a 6-311G** basis set was used to obtain the ground state geometry and vibrational frequencies of DPA. The harmonic frequencies were scaled with an empirical, basis dependent factor of 0.967 to consider for anharmonicities [4]. Intensities were calculated from the Raman activity S_i for a wavelength excitation of 785 nm at T=293.15 K [5], [6]. Raman spectra were convoluted with a Lorentzian with a full width at half maximum (FWHM) of 10 cm⁻¹. DFT calculations were performed using the Gaussian 09 program [7] and the Raman analysis using the GaussSum software [8].

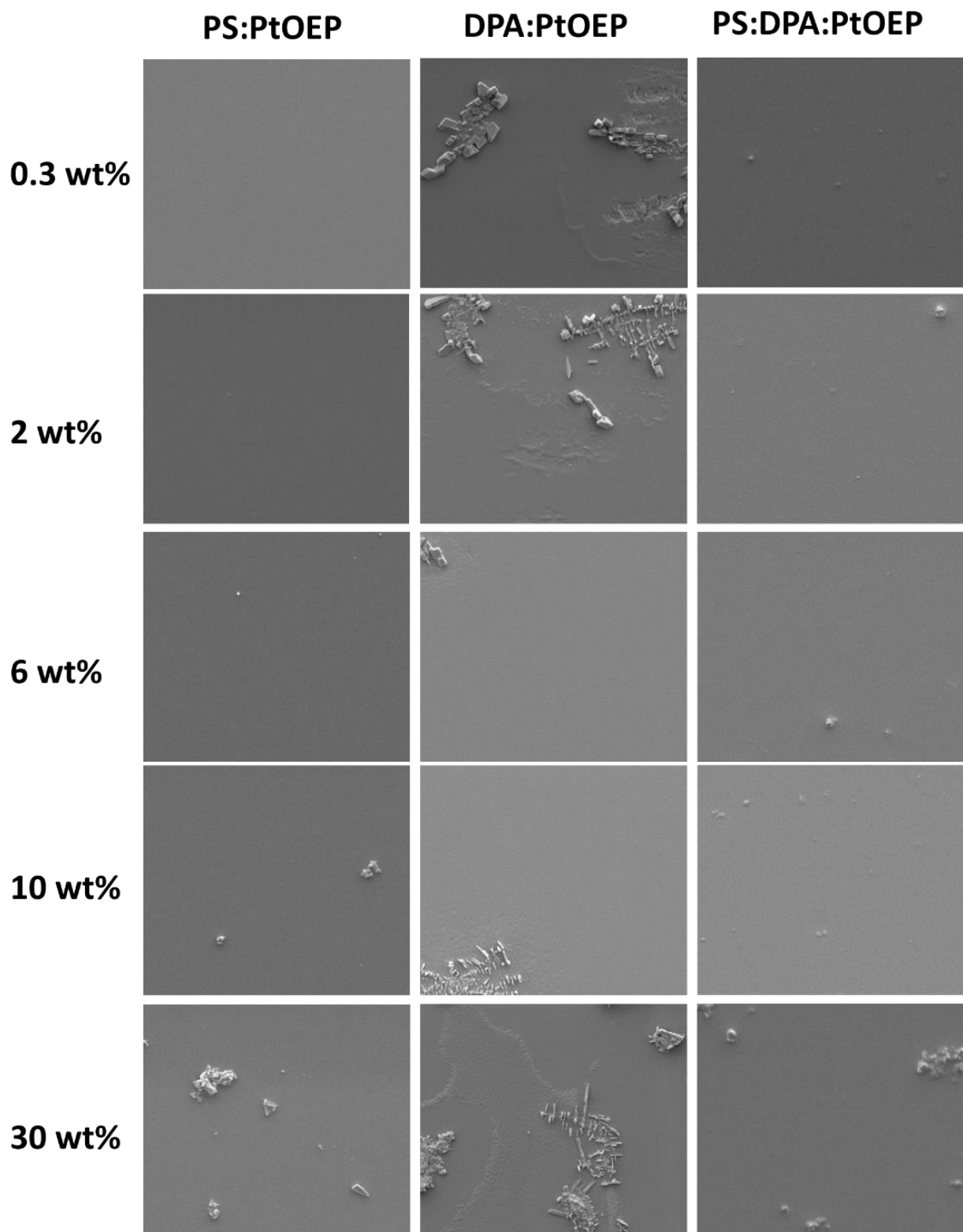


Figure S.1: Composition dependent SEM images (50 μm horizontal image length) of PS:PtOEP, DPA:PtOEP and PS:DPA:PtOEP films, as spin-coated from toluene solutions.

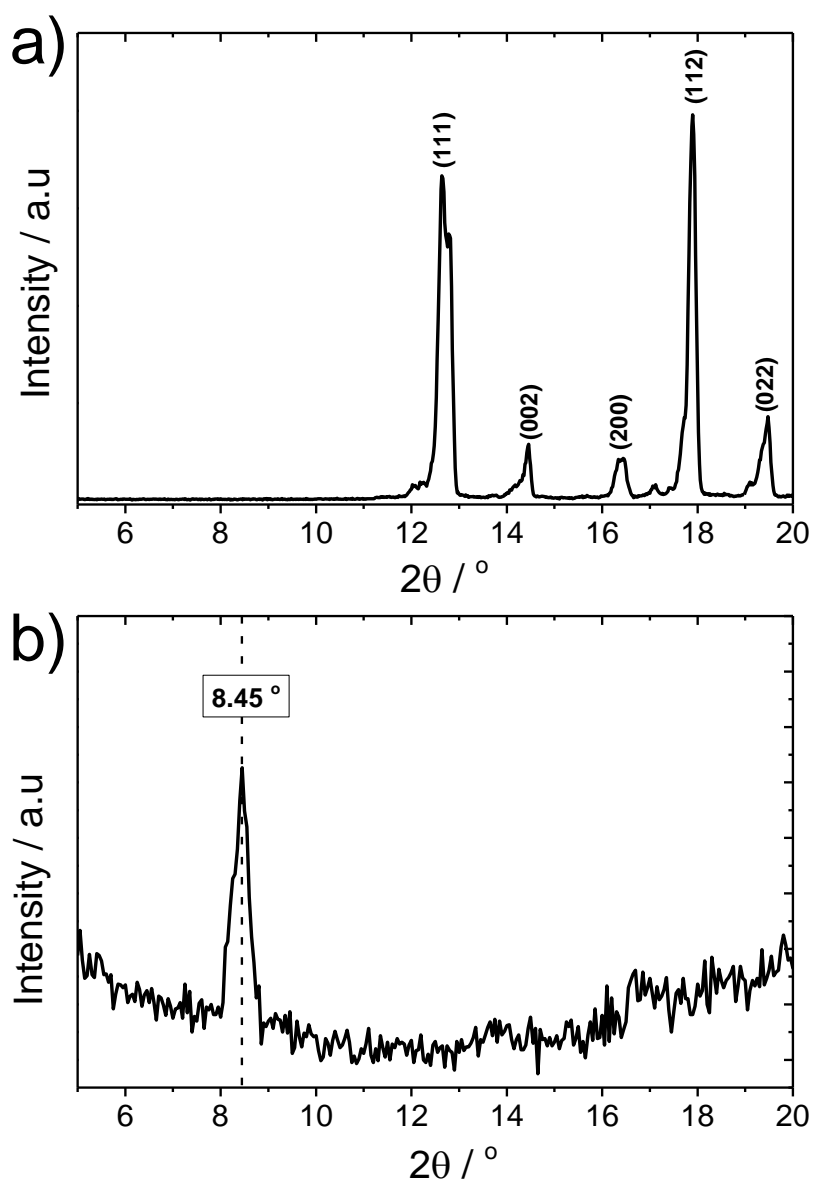


Figure S.2: a) Powder X-ray diffraction of DPA, b) grazing incidence X-ray diffraction of a thermally evaporated DPA layer on a glass/ITO/PEDOT:PSS substrate.

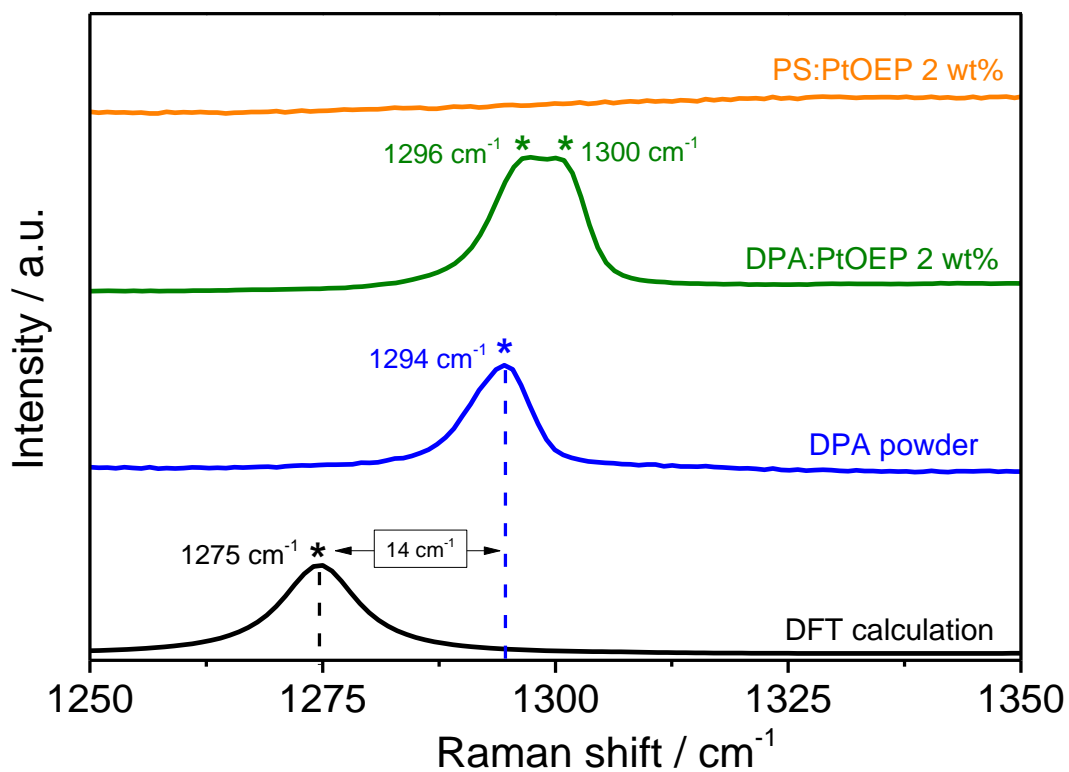


Figure S.3: Experimentally acquired Raman spectra of DPA powder form (blue line) and of spin-coated as-spun DPA:PtOEP 2 wt% (green line) and PS:PtOEP 2 wt% (orange line) films. In all cases the photoexcitation was at 785 nm. For reference purposes the theoretically calculated Raman spectrum of DPA in the gas phase (black line) is also displayed.

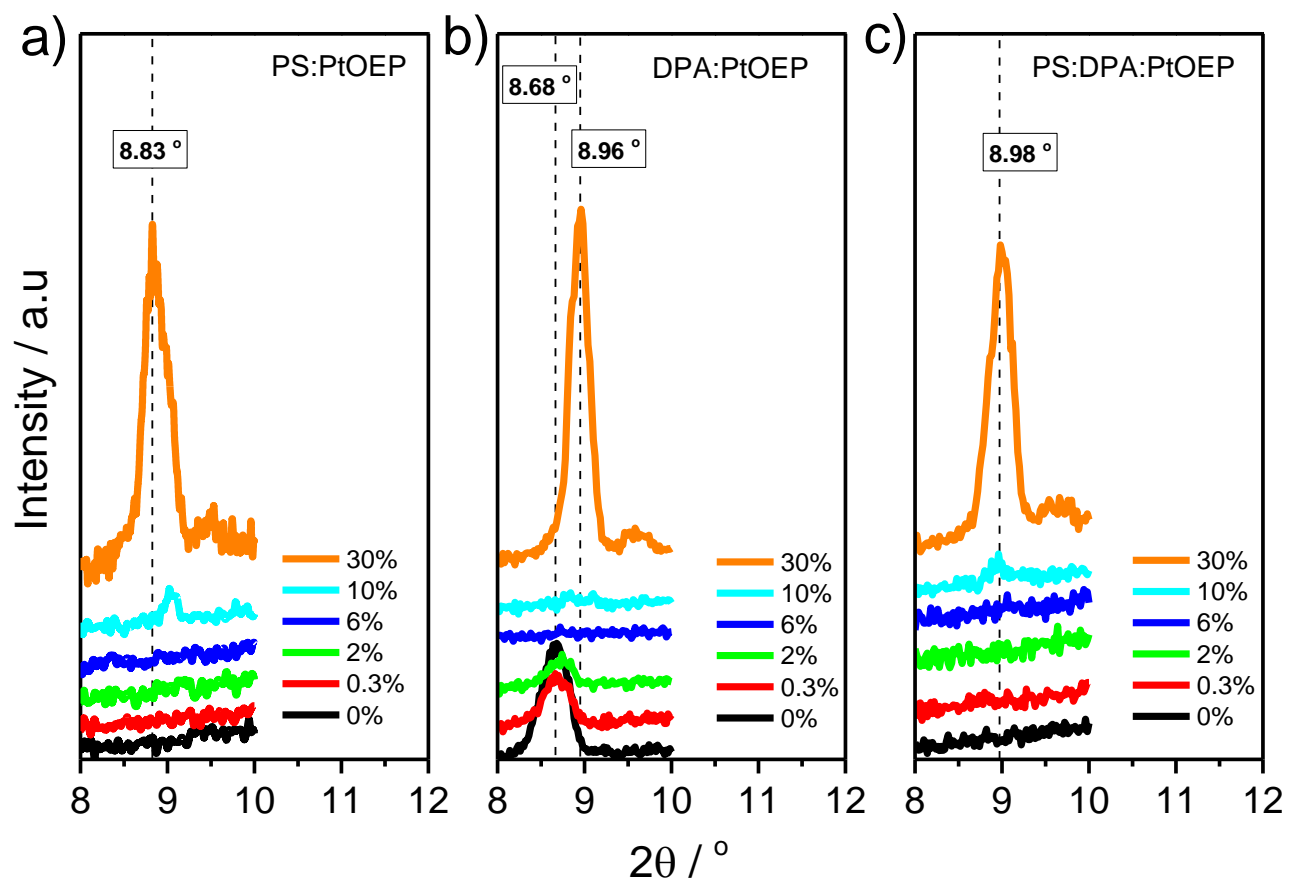


Figure S.4: Composition dependent GIXRD diffractograms of PS:PtOEP, DPA:PtOEP and PS:DPA:PtOEP films, as spin-coated from toluene solutions.

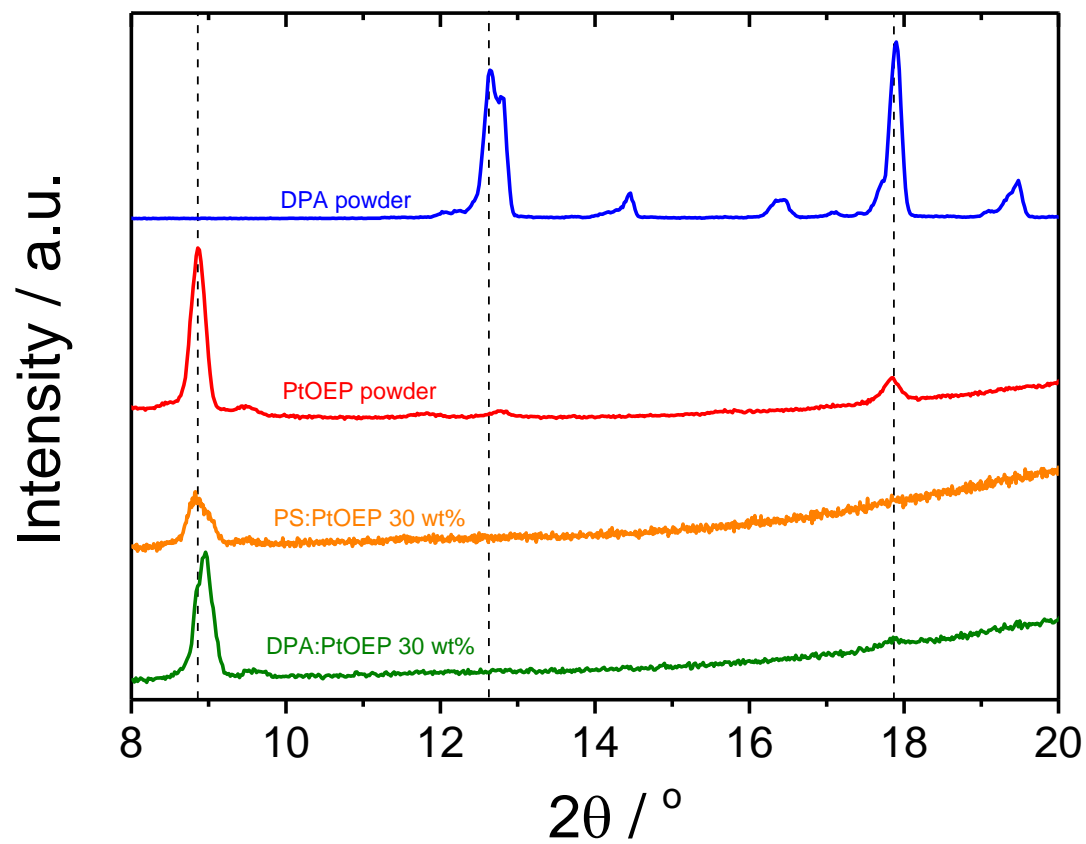


Figure S.5: GIXRD diffractograms of the PS:PtOEP 30 wt% (orange line) and DPA:PtOEP 30 wt% (green line) as compared with the XRD diffractograms of DPA (blue line) and PtOEP (red line) powders.

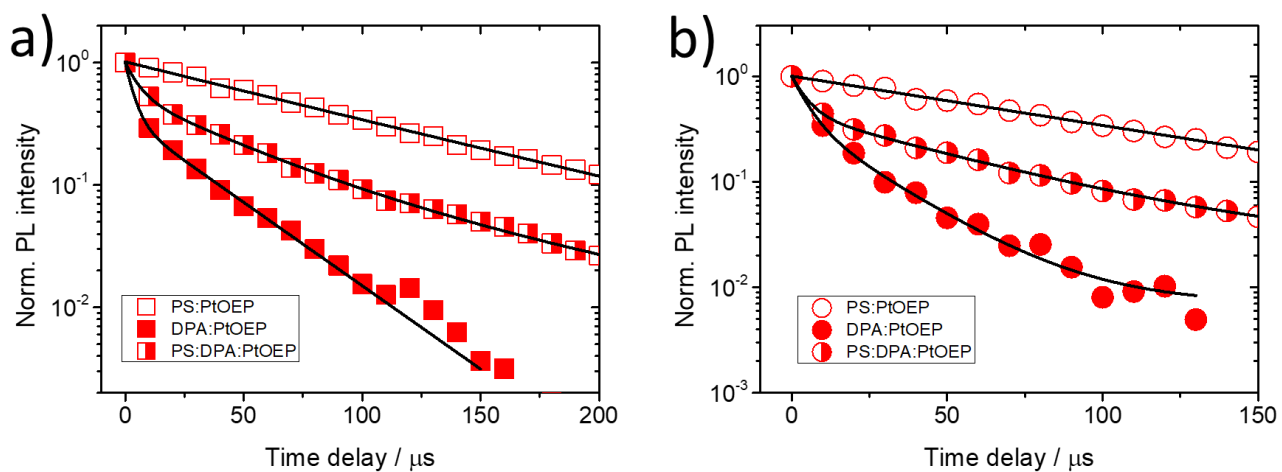


Figure S.6: Time-gated PL transients in the μs timescale at room temperature of a) PtOEP monomer phosphorescence at 644 nm (squares), and b) PtOEP triplet dimer phosphorescence at 780 nm (circles) for toluene spin-coated films of PS:PtOEP (open symbols), DPA:PtOEP (filled symbols) and PS:DPA:PtOEP (semi-filled symbols). In all cases the PL transients were acquired with a 10 μs gate window and a 10 μs gate step. Solid lines are exponential fits on the data. (see Table S.1 below)

Table S.1: Characteristic fitting parameters of triplet PtOEP exciton PL kinetics (644 nm) in the μs time scale at 180 K and at 290 K

| System | A ₁ | τ_1 (μs) | A ₂ | τ_2 (μs) | A ₃ | τ_3 (μs) | $\langle\tau\rangle$ (μs) |
|--------------|----------------|----------------------------|----------------|----------------------------|----------------|----------------------------|--|
| 180 K | | | | | | | |
| PS:PtOEP | 0.30 | 127 | 0.65 | 81 | - | - | 100 |
| DPA:PtOEP | 0.30 | 7 | 0.70 | 96 | - | - | 93 |
| PS:DPA:PtOEP | 0.35 | 40 | 0.30 | 94.5 | 0.30 | 3.5 | 75 |
| 290 K | | | | | | | |
| PS:PtOEP | 0.70 | 82 | 0.30 | 115 | - | - | 94 |
| DPA:PtOEP | 0.65 | 3.6 | 0.35 | 32 | - | - | 27 |
| PS:DPA:PtOEP | 0.40 | 42 | 0.45 | 5.5 | 0.15 | 110 | 71 |

Table S.2: Characteristic fitting parameters of triplet PtOEP dimer PL kinetics (780 nm) in the μs time scale at 180 K and at 290 K

| System | A ₁ | τ_1 (μs) | A ₂ | τ_2 (μs) | A ₃ | τ_3 (μs) | $\langle\tau\rangle$ (μs) |
|--------------|----------------|----------------------------|----------------|----------------------------|----------------|----------------------------|--|
| 180 K | | | | | | | |
| PS:PtOEP | 0.95 | 97 | - | - | - | - | 97 |
| DPA:PtOEP | 0.50 | 51 | 0.50 | 8.5 | - | - | 45 |
| PS:DPA:PtOEP | 0.15 | 152 | 0.50 | 3.0 | 0.5 | 52.5 | 96 |
| 290 K | | | | | | | |
| PS:PtOEP | 1.0 | 93 | - | - | - | - | 93 |
| DPA:PtOEP | 0.60 | 5 | 0.4 | 23 | - | - | 17 |
| PS:DPA:PtOEP | 0.40 | 50 | 0.55 | 5 | 0.05 | 310.0 | 152 |

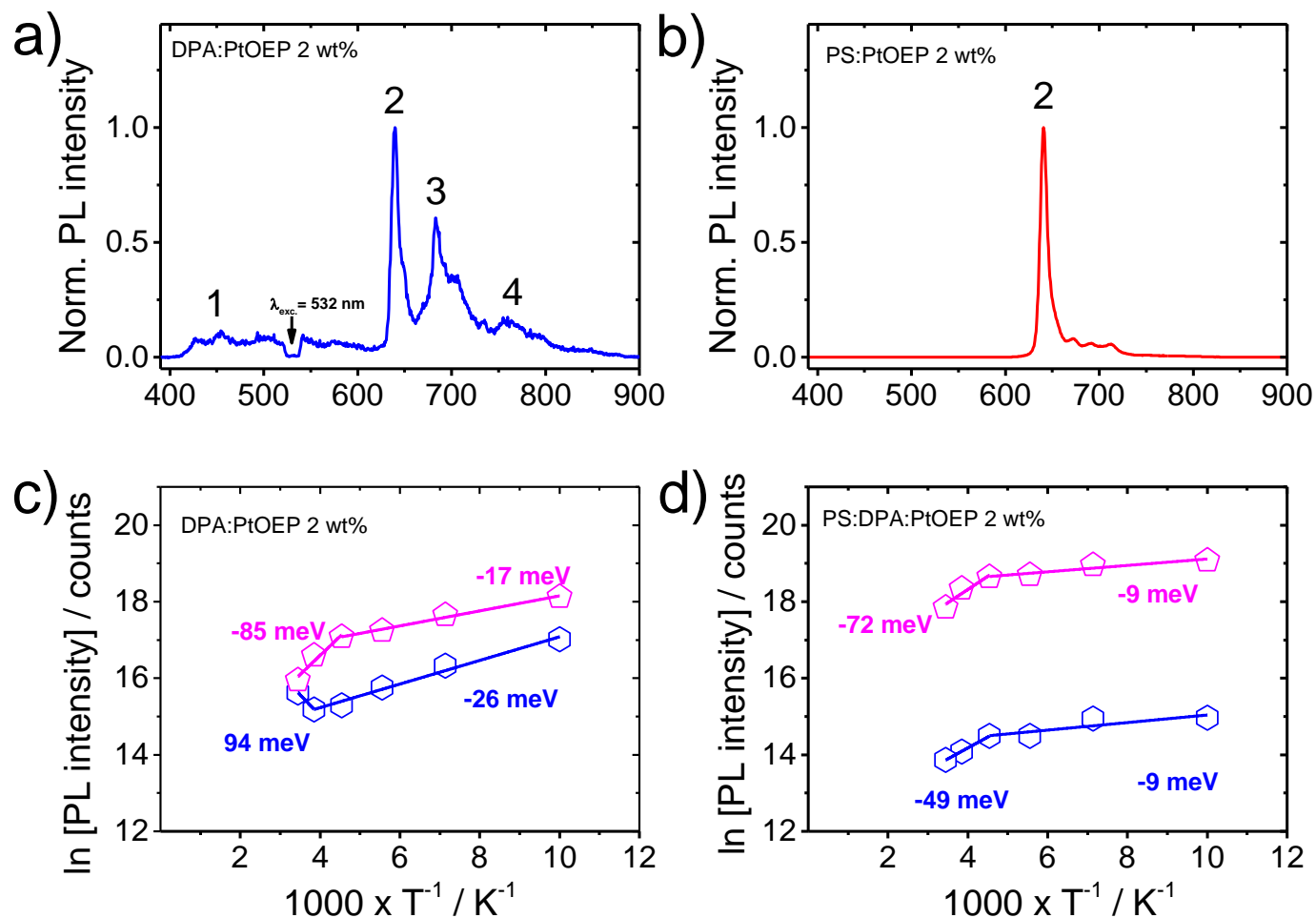


Figure S.7: Normalized time-gated PL spectra registered at 100 K for blend films of a) DPA:PtOEP 2 wt%) and b) PS:PtOEP 2 wt%, as developed by toluene. Both spectra correspond to the prompt luminescence of the films as acquired in the μ s time-scale (0 μ s time delay), after photoexcitation at 532 nm and when a gate-width of 10 μ s was used. The spectral positions of the PL intensities for the DPA TTA-UC luminescence, PtOEP phosphorescence, DPA phosphorescence and triplet PtOEP dimer emission signals are annotated in the spectra as 1, 2, 3 and 4, respectively. Temperature-dependent PL intensity of DPA TTA-UC delayed fluorescence (blue symbols) and DPA phosphorescence (magenta symbols) in c) DPA:PtOEP and d) PS:DPA:PtOEP films spin-coated from toluene. Solid lines in c) and d) are Arrhenius fits on the data.

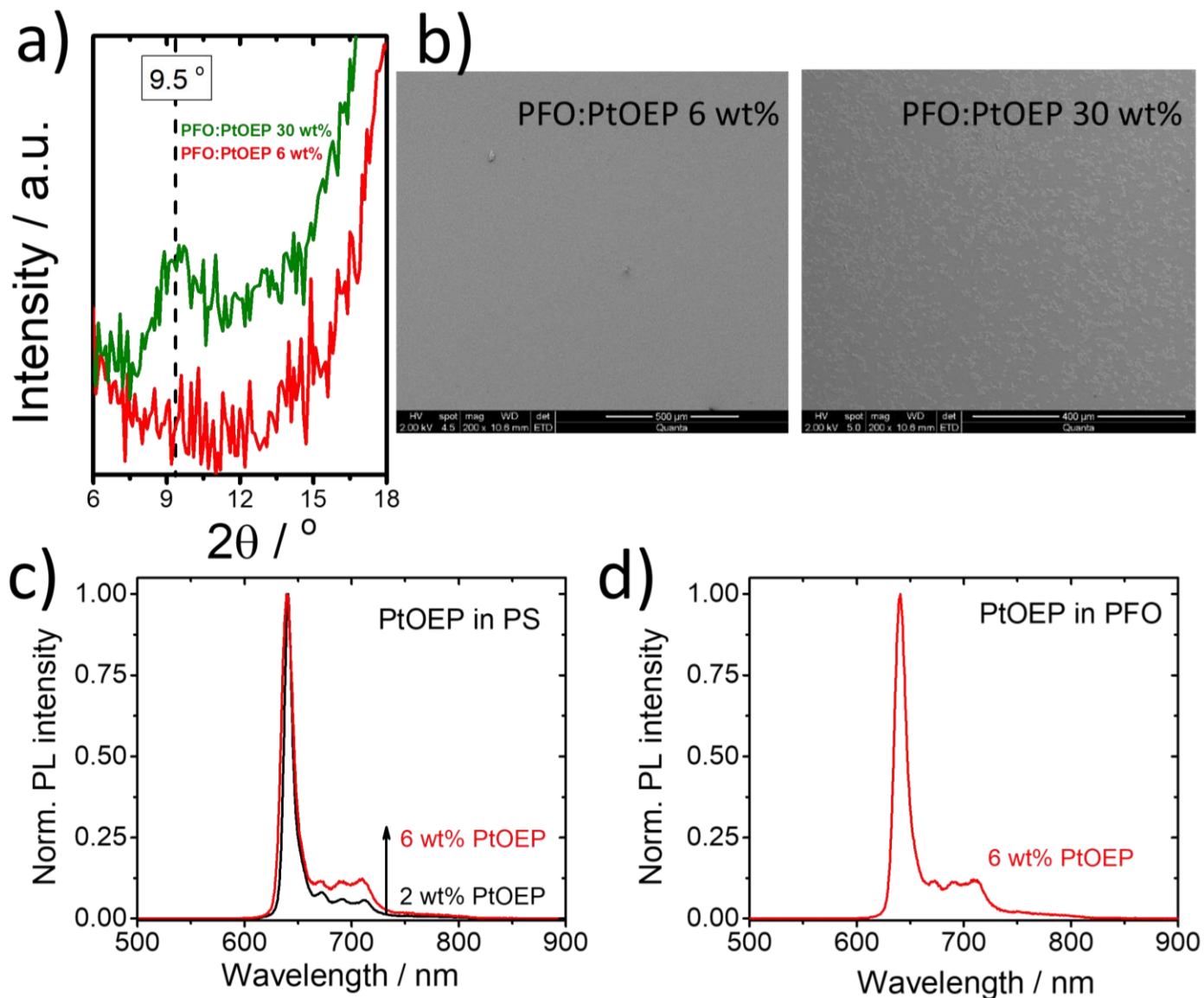


Figure S.8: a) GIXRD patterns of as-spun PFO:PtOEP films developed by toluene solutions with PtOEP content of 6 wt% (red line) and 30 wt% (green line). b) SEM images of the PFO:PtOEP films described in a). c) Time-gated PL spectra of as-spun PS:PtOEP films developed by toluene solutions with PtOEP content of 2 wt% (black line) and 6 wt% (red line). d) Time-gated PL spectra of as-spun PFO:PtOEP films developed by toluene solutions with PtOEP content of 6 wt% (red line). All PL spectra in c) and d) correspond to the prompt luminescence of the films at 100 K, as acquired in the μs time-scale ($0 \mu\text{s}$ time delay) after photoexcitation at 532 nm with a $10 \mu\text{s}$ gate-width.

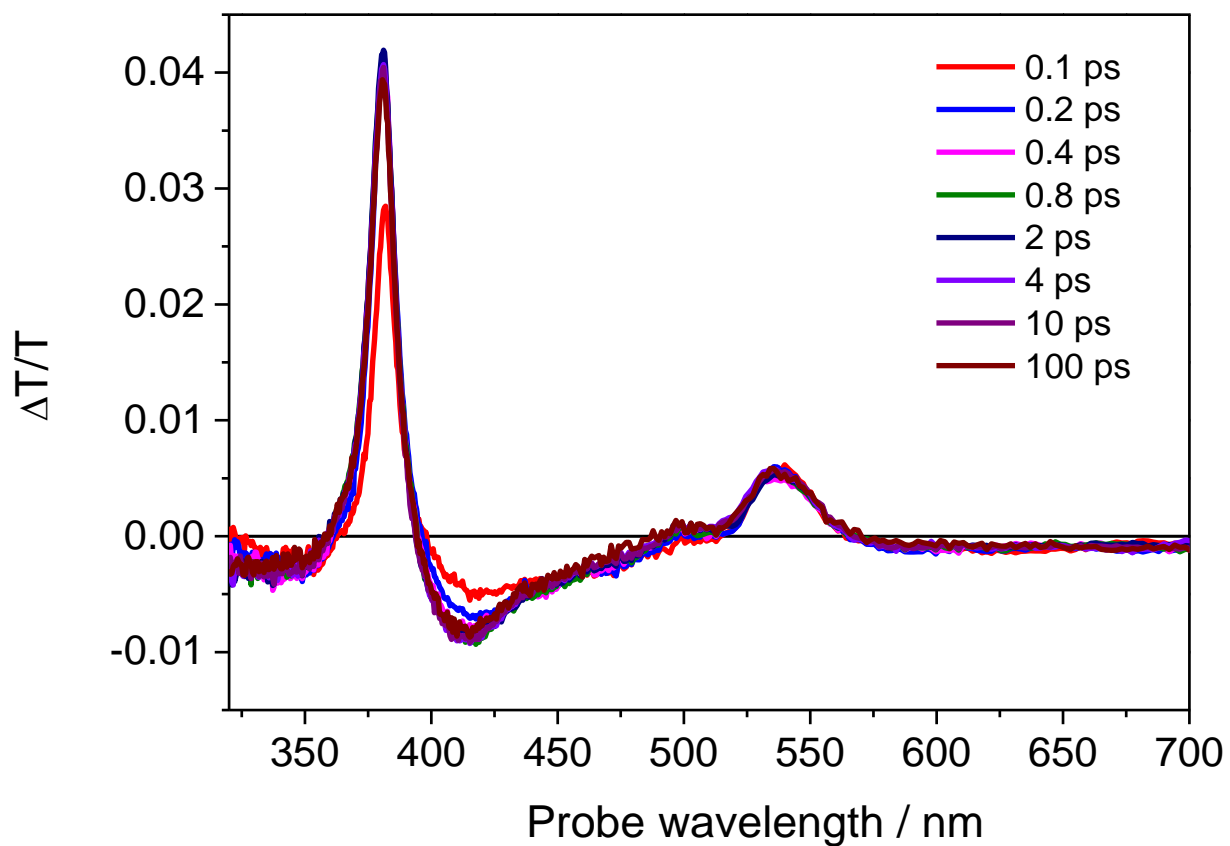


Figure S.9. Transient absorption ($\Delta T/T$) spectra of PS:PtOEP 6 wt% processed from toluene at different pump delays. Pump wavelength was at 540 nm.

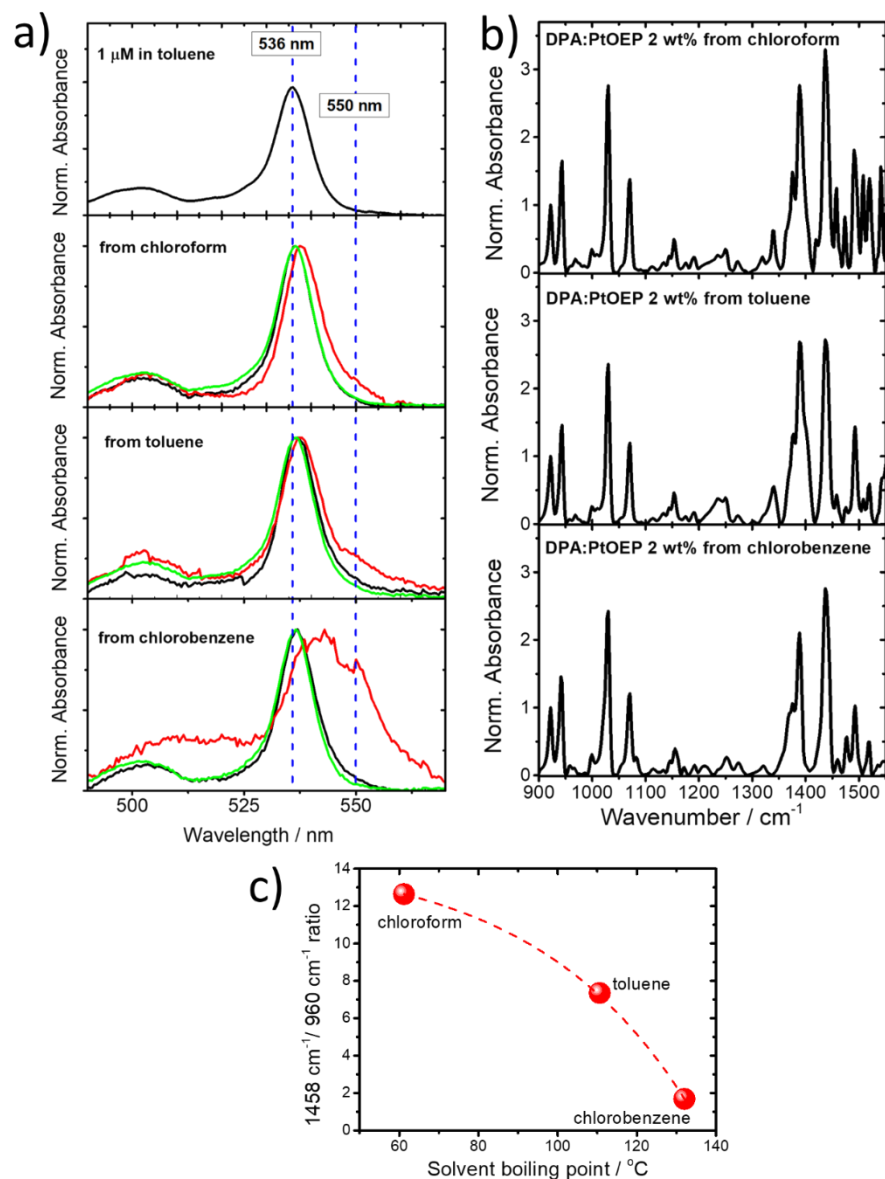


Figure S.10: a) Solvent-dependent UV-Vis absorption spectra of PS:PtOEP (black lines), DPA:PtOEP (red lines) and PS:DPA:PtOEP (green lines) films spin-coated from chloroform, toluene and chlorobenzene solutions. b) Solvent-dependent FT-IR spectra of DPA:PtOEP developed by toluene and chlorobenzene solutions c) Dependence of the the 1458 cm^{-1} /960 cm^{-1} vibration peak intensity ratio on the solvent boiling point; the red dash line is a guide to the eye. In all cases the PtOEP content was 2 wt%.

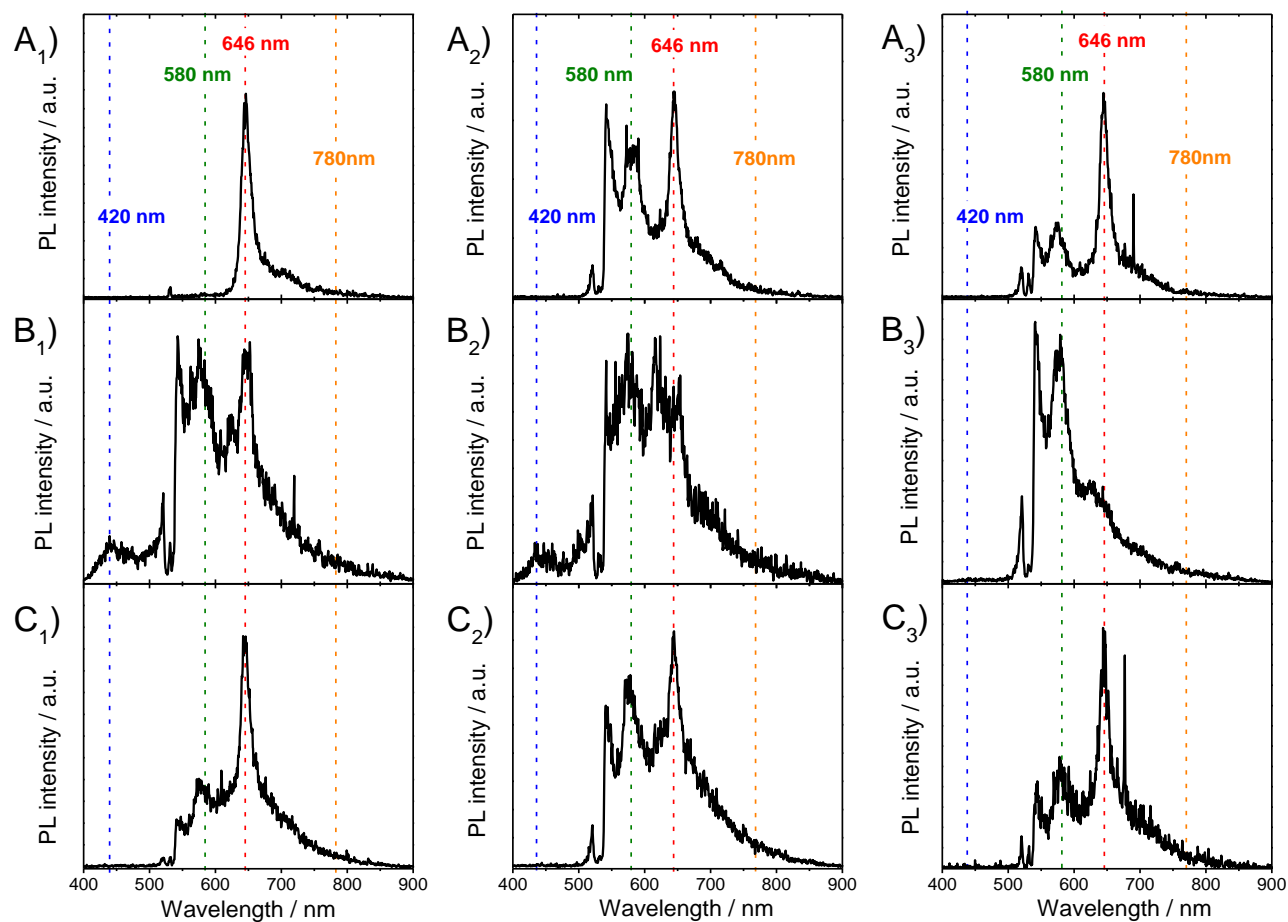


Figure S.11. Normalized time-gated PL spectra registered at 290 K for blend films of system A (PS:PtOEP 2 wt%), system B (DPA:PtOEP 2 wt%) and system C (PS:DPA:PtOEP 2 wt%) as developed by chloroform (1), toluene (2) and chlorobenzene (3). All spectra correspond to the prompt luminescence in the ns time-scale (0 ns time delay), after photoexcitation at 532 nm and when a gate-width of 10 ns was used.

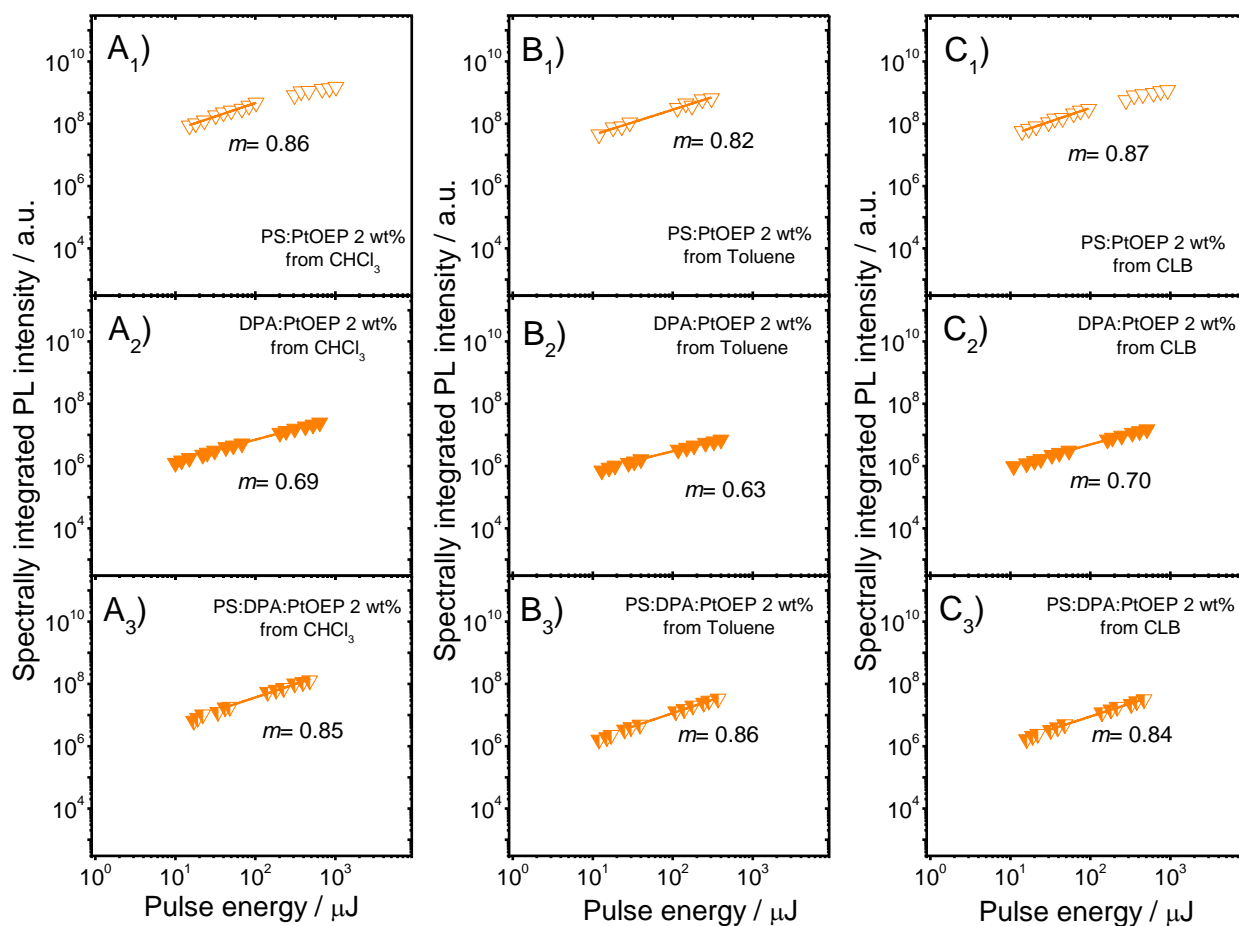


Figure S.12. Room temperature photoexcitation dependence of spectrally integrated PtOEP triplet dimer phosphorescence in blend films for PS:PtOEP 2 wt%, DPA:PtOEP 2 wt% and PS:DPA:PtOEP 2 wt% blend films, as developed by A) Chloroform (CHCl₃), B) Toluene and C) Chlorobenzene (CLB), after photoexcitation at 532 nm. The solid lines are fits on the data based on the functional power-law $I_{PL} \propto I_{exc}^m$ where the value of m is displayed in each of the graphs.

References

- [1] H. Goudarzi and P. E. Keivanidis, *J. Phys. Chem. C*, 2014, **118**, 14256–14265.
- [2] H. Goudarzi and P. E. Keivanidis, *ACS Applied Materials & Interfaces*, 2017, **9**, 845-857.
- [3] H. Goudarzi, S. Limbu, J. Cabanillas-González, V. M. Zenonos, J.-S. Kim and P. E. Keivanidis, *Journal of Materials Chemistry C*, 2019, **7**, 3634-3643.
- [4] NIST database: <http://cccbdb.nist.gov>
- [5] V. Krishnakumar, G. Keresztury, T. Sundius, R. Ramasamy, *Journal of Molecular Structure*, 2004, **702**, 9
- [6] G. Keresztury, S. Holly, G. Besenyei, J. Varga, Aiyang Wang, J.R. Durig, *Spectrochimica Acta Part A: Molecular Spectroscopy*, 1993, **49**, 2007
- [7] Gaussian 09, Revision B.01, M. J. Frisch, G. W. Trucks, H. B. Schlegel, G. E. Scuseria, M. A. Robb, J. R. Cheeseman, G. Scalmani, V. Barone, B. Mennucci, G. A. Petersson, H. Nakatsuji, M. Caricato, X. Li, H. P. Hratchian, A. F. Izmaylov, J. Bloino, G. Zheng, J. L. Sonnenberg, M. Hada, M. Ehara, K. Toyota, R. Fukuda, J. Hasegawa, M. Ishida, T. Nakajima, Y. Honda, O. Kitao, H. Nakai, T. Vreven, J. A. Montgomery, Jr., J. E. Peralta, F. Ogliaro, M. Bearpark, J. J. Heyd, E. Brothers, K. N. Kudin, V. N. Staroverov, T. Keith, R. Kobayashi, J. Normand, K. Raghavachari, A. Rendell, J. C. Burant, S. S. Iyengar, J. Tomasi, M. Cossi, N. Rega, J. M. Millam, M. Klene, J. E. Knox, J. B. Cross, V. Bakken, C. Adamo, J. Jaramillo, R. Gomperts, R. E. Stratmann, O. Yazyev, A. J. Austin, R. Cammi, C. Pomelli, J. W. Ochterski, R. L. Martin, K. Morokuma, V. G. Zakrzewski, G. A. Voth, P. Salvador, J. J. Dannenberg, S. Dapprich, A. D. Daniels, O. Farkas, J. B. Foresman, J. V. Ortiz, J. Cioslowski, and D. J. Fox, Gaussian, Inc., Wallingford CT, 2010.
- [8] N. M. O'Boyle, A. L. Tenderholt and K. M. Langner. *J. Comp. Chem.*, 2008, **29**, 839-845.